Silver(I) and Thioether-bis(pyrazolyl)methane Ligands: The Correlation between Ligand Functionalization and Coordination Polymer Architecture

CRYSTAL GROWTH & DESIGN

Article

pubs.acs.org/crystal

Silver(I) and Thioether-bis(pyrazolyl)methane Ligands: The Correlation between Ligand Functionalization and Coordination Polymer Architecture

Irene Bassanetti,[†] Corrado Atzeri, Dario Alberto Tinonin, and Luciano Marchiò*

Dipartimento di Chimica, Università degli studi di Parma, Parco Area delle Scienze 17/a, 43124 Parma, Italy

Supporting Information

ABSTRACT: This work examines the crystal structures of 15 Ag(I) complexes with thioether functionalized bis(pyrazolyl)-methane derivatives to rationalize the influence of the ligand on the formation of (a) coordination polymers (CPs), (b) oligonuclear (hexameric and dinuclear) complexes, and (c) mononuclear complexes. It was previously reported how this ligand class could generate microporous architectures with permanent porosity. Some ligand modifications could induce a cavity size modulation while preserving the same overall architecture. The bis(pyrazolyl)methane scaffold can be easily functionalized with various structural fragments; hence the structural outcomes were studied in this work using various ligand modifications and Ag(I) salts. In particular, six new ligand classes were prepared with the following features: (1) The steric hindrance on the pyrazole rings $L^{3,3'Me}$, $L^{5,5'Me}$, $L^{5,3'Me}$, L^{CF3}, and L^{Br} was modified. (2) The steric hindrance was reduced on the peripheral thioether group: L^{SMe}. (3) Finally, the presence of fluorine and bromine atoms in L^{CF3} and L^{Br} offered the possibility to expand the type of interaction with respect to the ligands based on hydrocarbon substituents (CH_3, phenyl, naphthyl). The effect of the anions was explored using different Ag(I) precursors such as $AgPF_6$, $AgBF_4$, $AgCF_3SO_3$, or $AgNO_3$. A comparison of the crystal structures allowed for the tentative identification of the type of substituents able to induce the formation of CPs having permanent porosity to include a symmetric and moderate steric hindrance on the pyrazolyl moieties (four CH_3) and an aromatic and preorganized thioether moiety. An asymmetric steric hindrance on the pyrazole groups led to the formation of more varied structural types. Overall, the most frequently reported structural motifs are the porous hexameric systems and the molecular chains.

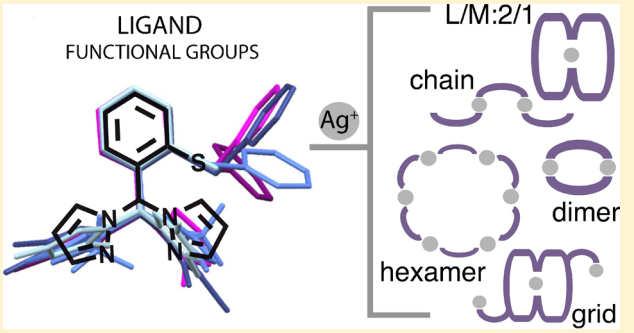

INTRODUCTION

Over the last three decades, the design of metal-based supramolecular assemblies has become one of the most intense research areas in chemistry and material science[1−7] due to the large number of potential applications of these materials, such as catalysis,[8,9] photochemistry,[10] luminescence,[11] sensing,[12] magnetism,[13,14] gas storage,[15−17] gas purification,[18,19] and medicine.[20] The ligand features and stereoelectronic characteristics of metal ions can control the arrangement of the supramolecular assemblies. The majority of transition metal ions usually exhibit a well-defined geometry (e.g., tetrahedral, square planar, or octahedral). In contrast, the geometry of d^{10} metal centers is typically dictated by steric factors, ensuring a greater coordination flexibility. Additional control over the resulting structural arrangement can be achieved by the use of multitopic ligands, which can bridge different metal ions to build flexible network structures. The mutual orientation of the donor atoms defines the ligand geometry as well as the coordinative directionality; the orientation has a profound influence on the overall geometrical structure.[1] These concepts are at play in the rational design in various architectures, such as metal organic frameworks (MOFs), coordination polymers (CPs), and supramolecular architectures, based upon extended metal−ligand interactions such as polyoxometallates (POMs) or networks based on supramolecular synthons.[21−24] Recent reviews have covered the conceptual distinctions between various types of metal based frameworks, in particular, between MOFs and CPs.[1,3,25,26] CPs commonly exhibit reversible coordination bonds and can be considered as dynamic synthons, which can assemble in various structural arrangements. CP architectures can be influenced by numerous factors including counterions, temperature, solvent systems, metal/ligand ratios, templates, and the coordination properties of the ligand and metal types.[27,28] CPs can also be prepared or processed in various ways to obtain nanostructured materials with potential applications in nanoelectronics[29,30] or in hybrid materials that can be incorporated into lipid membranes.[31] As far as the metal ion is concerned, the adaptable coordination geometry of Ag(I) allows for the use of silver cationic complexes as building blocks for the construction of

Received: April 1, 2016
Revised: May 3, 2016

DOI: 10.1021/acs.cgd.6b00506
Cryst. Growth Des. XXXX, XXX, XXX−XXX

coordination polymers.[32−37] Previous works investigated the coordination properties of thioether functionalized bis-(pyrazolyl)methane ligand systems (N_2S donors), which were able to generate CPs with metal ions such as Cu(I) and Ag(I).[38,39] Interestingly, it was found that in the presence of a specifically preorganized thioether-bis(pyrazolyl)methane ligand, Ag(I) could give hexameric and toroidal supramolecules (panels A and C in Figure 1) that self-assembled into diverse three-dimensional (3D) porous supramolecular architectures and microporous cavities as a function of the anion used (BF_4^-, PF_6^-, NO_3^-, and $CF_3SO_3^-$).[40] The employed type of ligand offered the possibility to functionalize the thioether moiety to modulate the porous properties of the resulting assemblies. In particular, ligands with bulky substituents led to a reduction in the size of some of the structural cavities. In one case, the interior of the cavities could be decorated with heteroatoms such as fluorine. Gas absorption measurements proved that the ligand bulkiness is directly correlated with the absorption properties of the resulting systems.[41] A large number of molecular structures based on the bis(pyrazolyl)methane scaffold were reported, in which bis(pyrazolyl)methane functionalization provided additional donor moieties (O, S, P) to the N_2 system or added specific linkers capable of generating extended multitopic ligands.[42−53] The scope of this work was to investigate the role of the bis(pyrazole)methane moiety on the structural arrangement of previously reported silver complexes (see panels A and C in Figure 1); thus various bis(pyrazolyl)methane scaffolds were prepared with different groups on the pyrazole rings, as shown in Scheme 1.

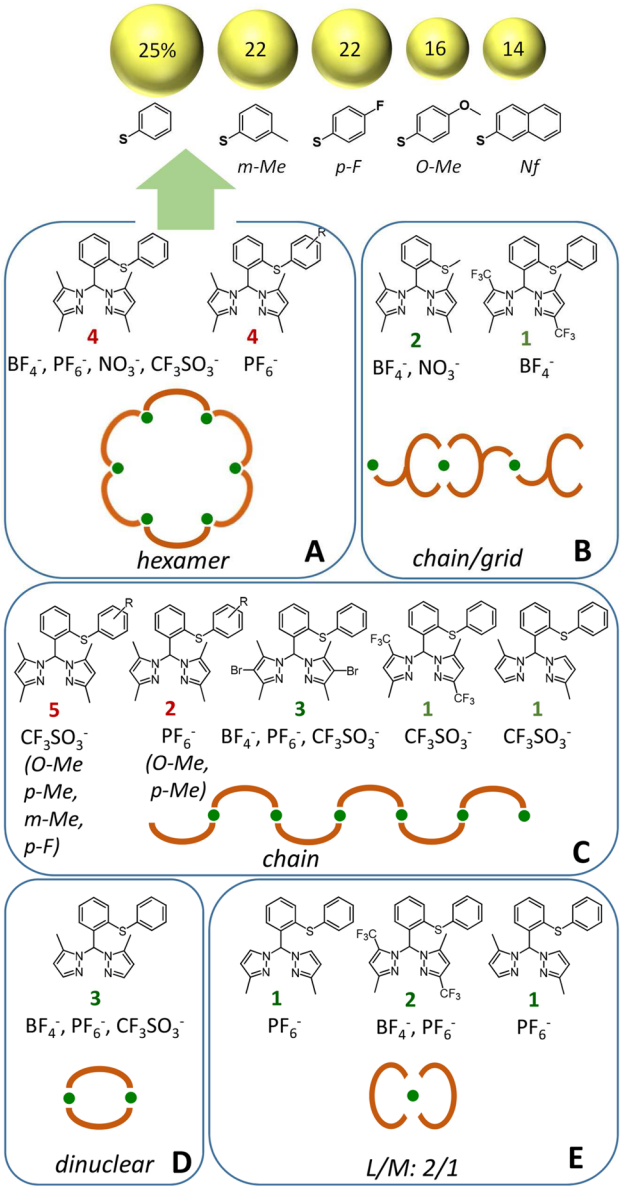

Figure 1. (A−E) Depiction of the structural variability of the thioether functionalized bispyrazolylmethane ligands with Ag(I) and different counteranions. The red number indicates previously reported structures, and green numbers indicate the structures reported in this work. The upper part of the picture shows the cavity dimensions (intra- and intercapsular) as a percentage of the unit cell volume for the $[Ag(L)]_6(PF_6)_6$ complexes.

Scheme 1. Molecular Structures of the Six Ligand Classes Described This Work[a]

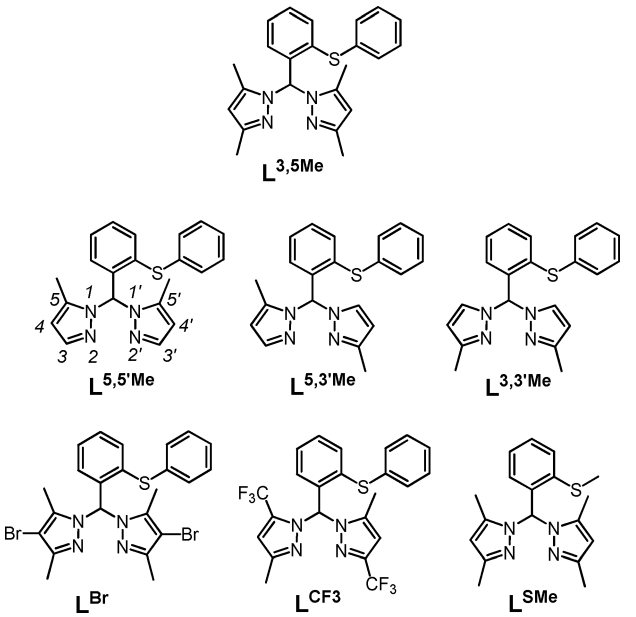

[a] $L^{3,5Me}$ was the parent ligand previously described.

In particular, the three isomers $L^{3,3'Me}$, $L^{5,5'Me}$, and $L^{5,3'Me}$ offered the possibility to investigate the steric hindrance role close to both the pyrazole nitrogen atoms. The L^{CF3} ligand was used to increase slightly the steric hindrance close to the N_2 system and to modify the electronic nature of the cavity surface in putative porous architectures. L^{Br} was chosen as a system exhibiting a moderate bulkiness on the pyrazole rings. When examining an expansion of the interactions occurring in these architectures, the bromine atoms of L^{Br} could also act as a halogen bond donor.[54] Moreover, with the aim of increasing the cavity size of potential porous architectures, the ligand L^{SMe} was prepared. L^{SMe} exhibits a limited steric hindrance of the ligand periphery, and it could provide hexameric building blocks with augmented porosity (see Figure 1). The molecular structures of the six classes of ligands with Ag(I) are used as a continuation of a previous study on the structural properties of Ag(I)-based CPs. The role of the counterion on coordination geometry, topology, and crystal packing was taken into consideration by using PF_6^-, BF_4^-, $CF_3SO_3^-$, and NO_3^-. A

DOI: 10.1021/acs.cgd.6b00506
Cryst. Growth Des. XXXX, XXX, XXX−XXX

comprehensive view of the structural variability obtained with these ligand classes, Ag(I) and anions is provided in Figure 1.

EXPERIMENTAL SECTION

Materials and Methods. All reagents and solvents were commercially available. 2-(Phenylthio)benzaldehyde and bis(3,5-dimethyl-1*H*-pyrazol-1-yl)methanone were prepared as reported elsewhere.[40] ^{1}H-NMR and ^{13}C-NMR spectra were recorded on a Bruker Advance 300 and 400 spectrometer using standard Bruker pulse sequences. Chemical shifts are reported in parts per million (ppm) referenced to residual solvent protons. Infrared spectra were recorded from 4000 to 700 cm^{-1} on a PerkinElmer FT-IR Nexus spectrometer equipped with a Thermo-Nicolet microscope. Elemental analyses (C, H, and N) were performed with a Carlo Erba EA 1108 automated analyzer. Electrospray ionization mass spectra (ESI-MS) were collected on a Micromass LCZ TOF electrospray ionization mass spectrometer. A capillary voltage of 3.0 V and a positive cone voltage of 50 V (ESI+ ion mode) were used. Samples (40 μL) were injected through direct infusion using a syringe pump at 10 μL/min, and the spectra were recorded in full scan analysis mode. The synthesis of the ligands and of the silver(I) complexes is reported in the Supporting Information.

Single Crystal X-ray Structures. Single crystal data were collected with a Bruker Smart APEXII area detector diffractometers (Mo Kα; λ = 0.71073 Å). Cell parameters were refined from the observed setting angles and detector positions of selected strong reflections. Data collection was performed with a 0.3° scan and with several series of exposure frames covering at least a hemisphere of the reciprocal space.[55] A multiscan absorption correction was applied to the data using the program SADABS.[56] The structures were solved by direct methods (SIR programs)[57] and refined with full-matrix least-squares (SHELXL-2014)[58] using the Wingx software package.[59] Selected geometric parameters are reported in Tables S1−S6 and Tables S7−S10 report the crystallographic data. Graphical material was prepared with the Mercury[60] 3.0 program. Thermal ellipsoids plots of the asymmetric units for all of the molecular structures are reported in the Supporting Information Figures S3−S7.

RESULTS AND DISCUSSION

Synthesis and Characterization. The synthesis of the ligands L^{Br}, L^{CF3}, $L^{3,3'Me}$, $L^{5,5'Me}$, $L^{5,3'Me}$, and L^{SMe} was performed as described in Scheme 2.

The N_2S donor set of the ligand described here is generated by treating substituted bis(pyrazolyl)ketones with functionalized (phenylthio)acetaldehyde using $CoCl_2$ hydrate as the catalyst and heating at 90 °C for 2 h and without solvent. Different pyrazoles were employed as the starting reagents. In particular, the pyrazole used comprised (i) bromine in position 4 together with methyl groups in positions 3 and 5, (ii) CF_3 and methyl groups in the 3, 5 positions, and (iii) a single methyl group. When using the pyrazole with a single methyl group and the pyrazole functionalized with a CF_3 group, different isomers were obtained. In particular, with a single methyl group, the synthesis led to the formation of three isomers, namely, $L^{3,3'Me}$, $L^{5,3'Me}$, and $L^{5,5'Me}$. Different purification steps via a chromatographic column were performed to isolate the three ligands from the reaction mixture. Different experimental conditions were attempted by changing the eluent mixture, the stationary phase (silica or alumina), or the column diameter. The best condition was identified with silica as stationary phase and hexane/ethyl acetate 8/2 as the eluent (see Figure S1). Nevertheless, the products $L^{5,3'Me}$ and $L^{5,5'Me}$ proved to be difficult to separate because they exhibited a very similar chromatographic behavior. After several chromatographic cycles it was possible to quantitatively purify $L^{3,3'Me}$ and isolate two pure fractions of $L^{5,3'Me}$ and $L^{5,5'Me}$, which were then used for the complexation studies. The purity of the three ligands was confirmed by ^{1}H NMR, as shown in Figure 2. Furthermore, different isomers can also be obtained when using the pyrazole with the CF_3 group. This is confirmed by the ^{1}H NMR spectrum of the crude product (Figure S3). Nevertheless, the isomer with the CF_3 groups in 3 and 5′ position (L^{CF3}) always showed a greater abundance over the other ones, which we did not attempt to purify. The complexes were prepared mixing equimolar amounts of the ligands with Ag(I) salts ($AgPF_6$, $AgBF_4$, $AgCF_3SO_3$, or $AgNO_3$) in acetone and in the air at room temperature. The purified products were investigated by means of ^{1}H NMR, which usually showed the presence of a single set of signals. Furthermore, the ESI-mass spectra showed the occurrence of $[Ag(L)]^+$ and in some cases also of the $[Ag(L)_2]^+$ species. This evidence points to the presence of potential dynamic equilibria in solution, which then resulted in the crystallization of different mononuclear, oligonuclear, and polynuclear structures as described below.

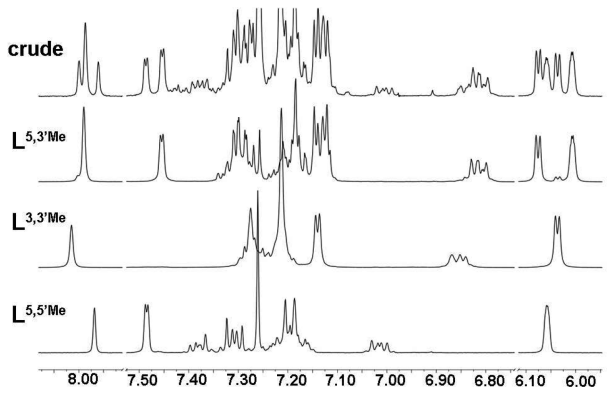

Figure 2. Stack between the aromatic region ^{1}H NMR spectra of the raw product and of the three purified ligands. In the raw product, the main impurity is represented by the aldehyde (reagent).

Scheme 2. Synthetic Route for the Preparation of the Ligands

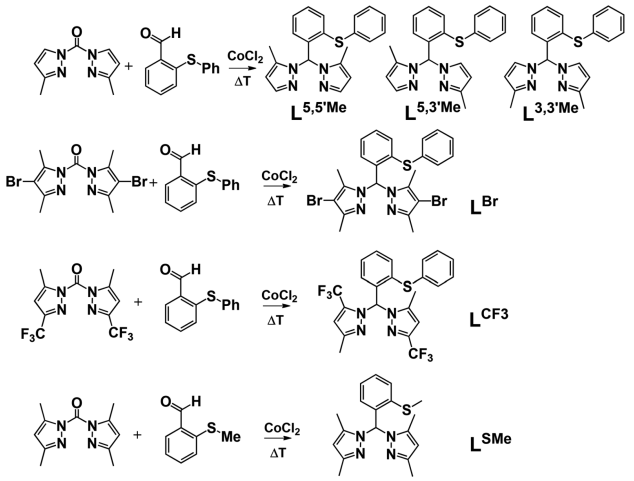

Crystals Structures of the Silver Complexes. *Molecular Chains.* Four ligand classes (L^{Br}, $L^{3,5Me}$, L^{CF3}, $L^{5,3'Me}$) exhibit the chain-like structural motif, which is the most represented among the silver complexes and comprise 12 overall structures

DOI: 10.1021/acs.cgd.6b00506
Cryst. Growth Des. XXXX, XXX, XXX−XXX

(Figure 1C). The complexes $[Ag(L^{Br})]_n(PF_6)_n$·acetone (**1**), $[Ag(L^{Br})]_n(BF_4)_n$·acetone (**2**), and $[Ag(L^{Br})]_n(CF_3SO_3)_n$·acetone (**3**) crystallize in the form of very similar molecular chains in the orthorhombic space group *Pbca*. This type of structure was previously found for ligand types ideally derived by $L^{3,5Me}$ and whose differences were represented by various functionalization of the peripheral thioether moiety (Figure 1).[41] For all of these compounds, the ligand acts as N_2 bidentate on a metal and bridges on another silver atom with the thioether group and with the central phenyl ring in a rigid geometry, as presented in Figure 3 and Figure S5. In these complexes, the

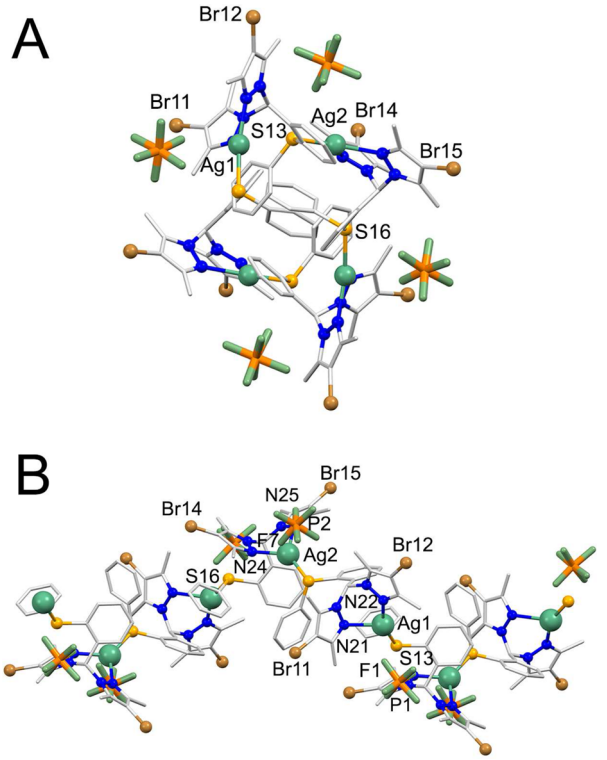

Figure 3. Molecular structure of $[Ag(L^{Br})]_n(PF_6)_n$·acetone (**1**) projected along the propagation direction of the molecular chain (A) and molecular chain side view (B).

asymmetric unit comprises a $[Ag(L^{Br})]_2(X)_2$ fragment (X = anion), as shown in Table S1. The metal is in a trigonal planar environment, which is slightly distorted toward the tetrahedral according to the presence of long contact with the fluorine atoms of BF_4^- or PF_6^- or the oxygen atoms of $CF_3SO_3^-$. In all structures, the metal is out of the trigonal plane to an extent that depends on the interaction degree with the anions. With PF_6^-, the metal lies out of the coordination plane of approximately 0.16−0.17 Å, whereas with BF_4^-, it lies out of approximately 0.17−0.22 Å. With $CF_3SO_3^-$, the metal lies out of 0.23−0.24 Å in agreement with the presence of a moderately short Ag−O contact (2.52 and 2.57 Å). The torsion angles (described as the angle between the bipyrazolyl scaffold and the phenyl linker) τ in Scheme 3 varies in the 0.0/−3.9° range, confirming a conserved ligand conformational rigidity among the three complexes. The structures present a π stacking between the pyrazole ring and the peripheral phenyl ring with distances that vary in the 3.3−3.5 Å range. These molecular chains exhibit a helical arrangement; both the left-handed and the right-handed directions are present in the crystal packing

Scheme 3. Torsion Angle Used to Describe the Conformational Rigidity of the Ligands

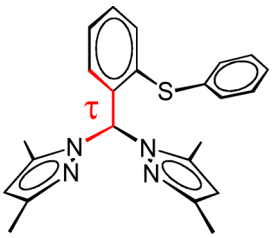

according to the fact that the structures are centrosymmetric. The exterior of the chains is defined by alternate anions and pyrazole rings, whereas those in the interior are located in the peripheral aromatic moieties of the thioether fragments. Contrary to the toroidal hexamers described in previous works,[40,41] the crystal packing of **1**−**3** does not exhibit any cavity with permanent porosity, even though acetone crystallization molecules are present. The steric profile of L^{Br} is slightly greater than that of $L^{3,5Me}$, according to the large size of bromine and the long C−Br bond distance (approximately 1.9 Å). This moderate increase of the steric hindrance on the 4-pyrazole position may be the main reason that hinders the formation of hexameric structures. In fact, by inspecting the structures of the parent compounds $[Ag(L^{3,5Me})]_6(BF_4)_6$ and $[Ag(L^{3,5Me})]_6(BF_4)_6$,[40] it appears that the additional presence of a bromine atom as in L^{Br} could provide some steric interference between adjacent and symmetry related molecules.

The molecular structure of $[Ag(L^{CF3})]_n(CF_3SO_3)_n$ (**4**) is reported in Figure 4. The ligand L^{CF3} bridges between two metal centers with the N_2 system on one side and the thioether group on the opposite side. The oxygen atom of a triflate anion completes the tetrahedral coordination of the metal center. The most notable difference with the previously described structures exhibiting the L^{Br} ligand is in the arrangement of the peripheral phenyl ring, which in **4** is not stacked above one of the pyrazole

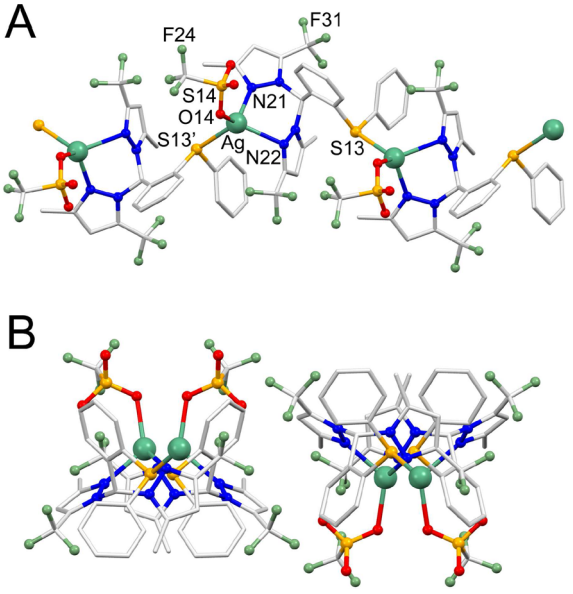

Figure 4. Molecular structure of $[Ag(L^{CF3})]_n(CF_3SO_3)_n$ (**4**) (A). Portion of the crystal packing as viewed along the *c* axis; two molecular chain are depicted (B). Hydrogen atoms were removed for clarity. Symmetry code ′ = 3/2 − *x*; *y*; 1/2 + *z*.

DOI: 10.1021/acs.cgd.6b00506
Cryst. Growth Des. XXXX, XXX, XXX−XXX

moieties as found with L^{Br}. This new conformation is likely a consequence of the steric hindrance caused by the CF_3 residues on the pyrazole rings belonging to the same ligand. To minimize the steric repulsion, the phenyl moiety is positioned above one of the CH_3 groups. The rigidity of the central phenyl ring is nevertheless preserved, as the τ angle is 2.9° (Scheme 3). The ligand conformation implies a different orientation of the lone pairs of sulfur; consequently, a different chain-like structure is formed. Interestingly, the peripheral phenyl interacts with the pyrazole ring of a symmetry related ligand, conserving the energetically favorable π stacking as found for the structure with L^{Br}. A possible consequence of the thioether organization is a significant lengthening of the Ag−S bond (2.62 Å) that is compensated for by a stronger interaction with the triflate anions yielding a relatively short Ag−O bond (2.31 Å).

A different type of molecular chain is observed for the complex $[Ag_2(L^{5,3'Me})]_n(CF_3SO_3)_{2n}\cdot 2CH_2Cl_2$ (**5**) where the metal ligand ratio is 2:1 even though the synthesis was performed with a 1:1 stoichiometry, as presented in Figure 5. In this complex, the ligand $L^{5,3'Me}$ adopts a conformation similar to that observed for the L^{Br} system, having the peripheral aromatic ring stacked above the 5-Me functionalized pyrazole ring. The absence of the 3′-Me group has an important consequence for the donor properties of this ligand. In fact, the N(21) nitrogen atom is devoid of significant steric hindrance; therefore, it can interact with two silver atoms in a bridging mode. Moreover, Ag(1) exhibits a distorted tetrahedral coordination achieved by two nitrogen atoms, a bridging sulfur atom of a symmetry related ligand, and an oxygen atom of a triflate anion O(15). The Ag(2) metal also exhibits a distorted tetrahedral geometry achieved by three oxygen atoms from three different triflate anions (two of them centrosymmetrically related). Ag(2) also interacts with the central aromatic ring of the ligand, giving rise to a metal-π interaction with the shortest distance observed between Ag(2) and C(33) (3.11 Å). Because of this latter interaction, there is a slight rotation of the central phenyl ring with respect to the bis(pyrazole) scaffold, and the τ angle is approximately 16.6°. From a different perspective, the structural arrangement of **5** can be viewed as a molecular chain that involves the ligand, the Ag(1), and a triflate anion. An additional Ag(2)-triflate fragment can easily interact with the N(21) bridging nitrogen according to the limited steric hindrance on this donor atom. Additionally, Ag(1) and Ag(2) give rise to an argentophilic interaction with a metal−metal distance of 3.173(1) Å. The Ag(2)-triflate fragment links together two molecular chains with this second triflate anion that bridges on the Ag(1) via the O(35) oxygen atom, producing an overall supramolecular grid, which is parallel to the *bc* crystallographic plane, as shown in Figure 5. Dichloromethane molecules of crystallization are allocated in the interstices of these layers.

Dinuclear Structures. When using the ligand $L^{5,5'Me}$, the structures of the silver complexes present a different arrangement. In fact, the three complexes $[Ag(L^{5,5'Me})]_2(PF_6)_2\cdot 2CH_2Cl_2$ (**6**), $[Ag(L^{5,5'Me})]_2(BF_4)_2\cdot CH_2Cl_2$ (**7**), and $[Ag(L^{5,5'Me})]_2(CF_3SO_3)_2$ (**8**) crystallize in a dinuclear form, but they can be grouped in two classes according to the different type of atoms involved in the metal coordination. In particular, in **6** the ligand acts as a N_2 bidentate on a metal center, and it interacts on a second silver atom with the thioether group. Within the dinuclear unit, there are two identical, very long contacts between the silver atoms and the symmetrically related

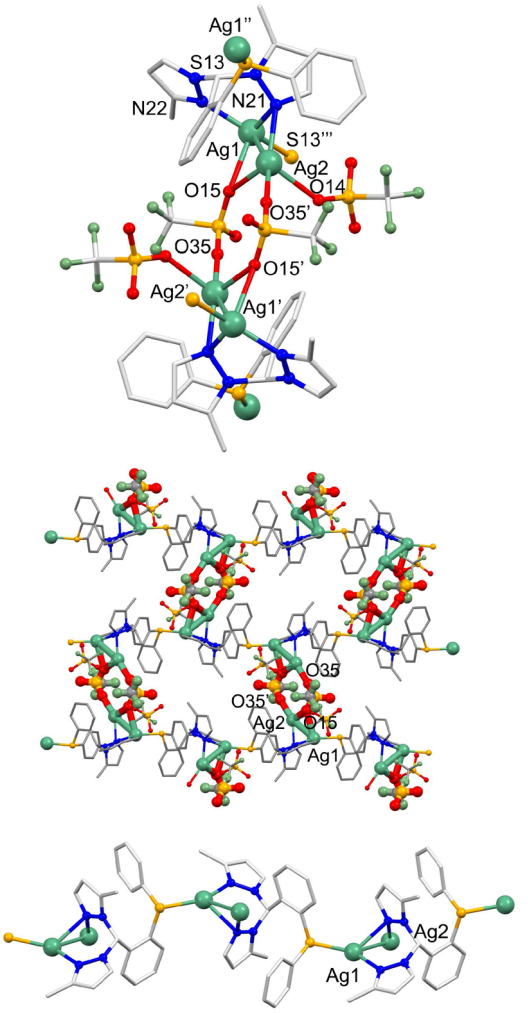

Figure 5. Molecular structure of $[Ag_2(L^{5,3'Me})]_n(CF_3SO_3)_{2n}\cdot 2CH_2Cl_2$ (**5**) highlighting the bridging triflate anions (top). Depiction of the supramolecular layers generated by the triflate bridges (middle) and of the molecular chain (bottom). Hydrogen atoms and solvent molecules of crystallization were removed for clarity. Symmetry codes: ′ = 1/2 − *x*; 1/2 − *y*; 1 − *z*, ′′ = 1/2 − *x*; 1/2 + *y*; 1/2 − *z*, ′′′ = 1/2 − *x*; *y* − 1/2, 1/2 − *z*.

N(22) atoms (2.993(3) Å). As a consequence, the silver atoms exhibit a distorted trigonal planar geometry (Figure 6) with the metal that lies out of the trigonal plane of 0.22 Å and is directed toward the N(22) nitrogen atom. The thioether is oriented on the same side of the N_2 binding moiety. The resulting ligand coordination mode is not typically observed for this ligand class and forces the central phenyl ring to adopt a slightly less favorable geometry than the remainder of the structures presented here. In particular, the torsion angle τ is 19°, which is significantly greater than the other structures reported. As far as the crystal packing is concerned, the dinuclear units assemble in supramolecular chains according to the presence of sulfur-π (3.46 Å) and $\pi-\pi$ (3.46 Å) stacking between the peripheral aromatic rings of adjacent molecules, illustrated in Figure 6A.

The complexes **7** and **8** present a dinuclear structure with the ligand that behaves as a bridging N_2 donor on two metal centers. In these two complexes, the thioether does not participate in the metal binding and is oriented as found in the great majority of the structures with a τ_1 of −4.6/1.7° and

DOI: 10.1021/acs.cgd.6b00506
Cryst. Growth Des. XXXX, XXX, XXX−XXX

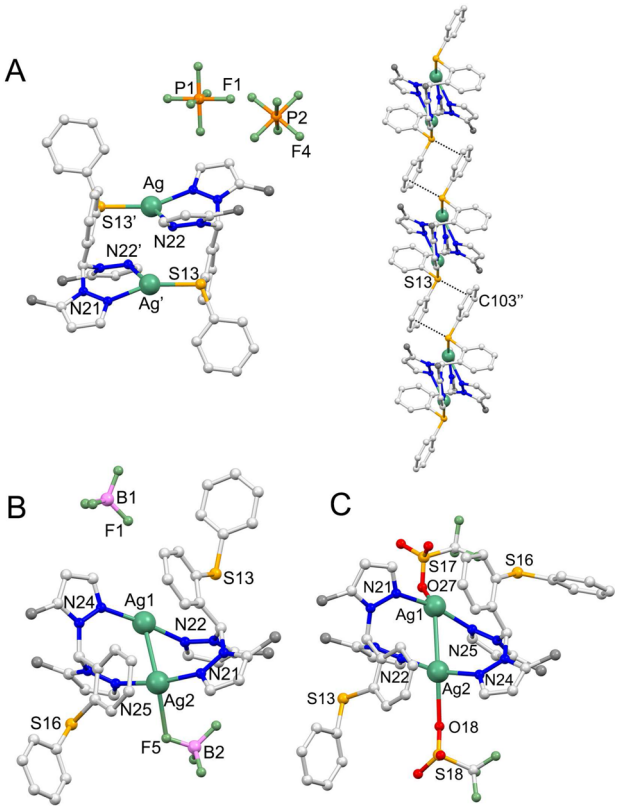

Figure 6. (A) Molecular structure of $[Ag(L^{5,5'Me})]_2(PF_6)_2{\cdot}2CH_2Cl_2$ (**6**) (left) together with the π stacking between the peripheral phenyl rings and portion of the supramolecular chain (right). (B) Molecular structure of $[Ag(L^{5,5'Me})]_2(BF_4)_2{\cdot}CH_2Cl_2$ (**7**). (C) Molecular structure of $[Ag(L^{5,5'Me})]_2(CF_3SO_3)_2$ (**8**). The hydrogen atoms and the solvent of crystallization were omitted for clarity. Symmetry codes: $' = -x; 1 - y; -z$, $'' = -1/2 - x; 3/2 - y; -z$.

−7.5/11.2°. The silver atom has a linear geometry, which is distorted by the interactions with the fluorine atom (from a disordered BF_4^- anion) or the oxygen atom (from a monodentate $CF_3SO_3^-$ anion), Figure 6. Another notable difference with the structures of **6** is the occurrence of an argentophilic interaction between the two silver atoms. This is supported by the presence of short contacts between the metal atoms of 2.94 Å in **7** and 3.11 Å in **8** and is significantly shorter than the vdW radii sum (3.44 Å).

The ligand $L^{5,5'Me}$ is conceptually derived by the parent compound $L^{3,5Me}$ (Scheme 1) by removing two methyl groups adjacent to the nitrogen donor atoms. This modification concurs to remove considerable steric hindrance on the donor functions of the ligands, thus favoring the approach of two ligand/metal systems and the formation of a dinuclear species.

Molecular Structures with M:L 1:2 Stoichiometry. Despite the use of a 1:1 M:L stoichiometry during the synthesis, some ligands yielded complexes with a M:L 1:2 stoichiometry, namely, $[Ag(L^{3,3'Me})_2](PF_6){\cdot}2$acetone (**9**), $[Ag(L^{5,3'Me})_2](PF_6){\cdot}CH_2Cl_2$ (**10**), $[Ag(L^{CF3})_2](PF_6)$ (**11**), and $[Ag(L^{CF3})_2](BF_4){\cdot}CH_2Cl_2$ (**12**), Figure 7. The structures are presented and the reasons rationalized here that underlie this occurrence. By inspecting the coordination environment of the four complexes, there is a modulation of the geometry that varies between the distorted tetrahedral and the linear one. The complexes having the $L^{3,3'Me}$ and $L^{5,3'Me}$ ligand exhibit a distorted tetrahedral geometry with two bidentate N,N′ ligand

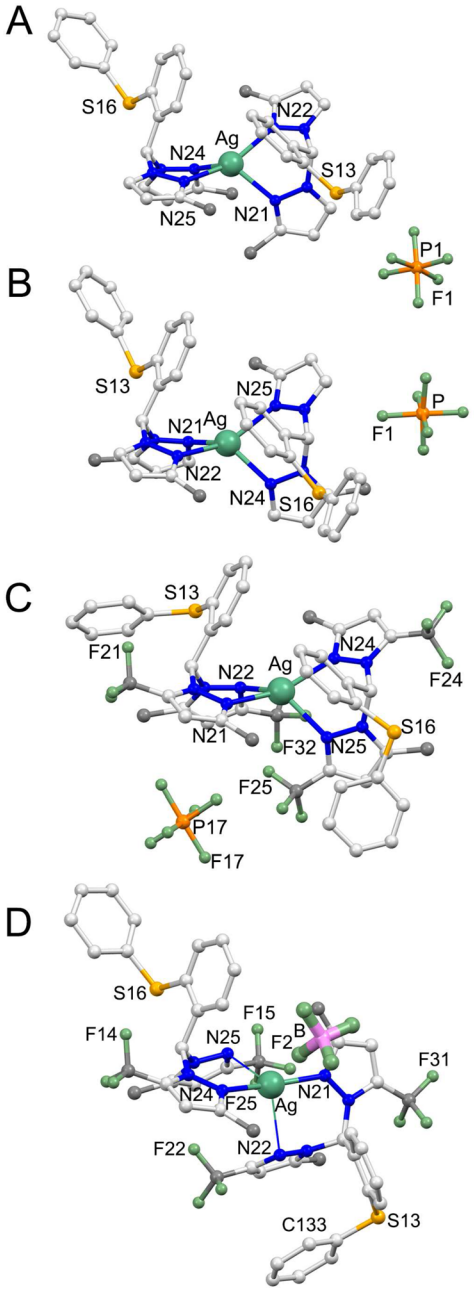

Figure 7. (A) Molecular structures of $[Ag(L^{3,3'Me})_2](PF_6){\cdot}2$acetone (**9**). (B) Molecular structure of $[Ag(L^{5,3'Me})_2](PF_6){\cdot}CH_2Cl_2$ (**10**). (C) Molecular structure of $[Ag(L^{CF3})_2](PF_6)$ (**11**). (D) Molecular structure of $[Ag(L^{CF3})_2](BF_4){\cdot}CH_2Cl_2$ (**12**) (D). Disordered anions, solvent molecules of crystallizations, and hydrogen atoms were removed for clarity. The carbon atoms of the functional groups of the pyrazole rings are highlighted in dark-gray.

and four nearly equivalent Ag−N distances (range 2.31−2.35 Å, Table S4, Figure 7A,B). Oppositely, **12** shows a relatively linear geometry because Ag−N(21) and Ag−N(24) are markedly shorter (2.18 and 2.19 Å) than the other two Ag−N distances (2.61 and 2.68 Å) and the angle N(21)−Ag−N(24) approaches 180°. An intermediate type of geometry, between the linear and the tetrahedral, is more evident in the complex **11**. In fact, the Ag−N(21) and Ag−N(24) distances are significantly shorter (2.32 and 2.34 Å) than the Ag−N(22) and Ag−N(25) (2.42 and 2.43 Å), but the difference is not as pronounced as in **12**. Additionally, in this case, the N(21)−Ag−N(24) angle (156°)

DOI: 10.1021/acs.cgd.6b00506
Cryst. Growth Des. XXXX, XXX, XXX−XXX

points to a distortion toward the linearity of the complex. Interestingly, in the complexes with the L^{CF3} ligand, the longest Ag−N bond distances are observed for the nitrogen atom close to the CF_3. This observation can be readily explained by taking into account the electron withdrawal effect exerted by the CF_3 residue on the nitrogen atom, thus reducing the donor capability of its lone pair. The τ angle of the central phenyl ring is −12.7/5.5 for **11**, −3.6/5.7 in **9**, and −1.7/7.6 in **10**. In **12**, one of the ligand exhibits a τ angle of −11.9°; however, for the second ligand, τ is of −31.5°, which is considerably greater than all of the structures presented in this work. This large deviation is a consequence of the steric hindrance between the CF_3 group and the peripheral phenyl ring, which exchanges a $\pi-\pi$ interaction with the pyrazole moiety. The closest contact is between the N(22) and C(133) atoms (3.42 Å, see Figure 7). In all structures, the thioether group is not involved in any interaction with the metal centers.

Molecular Structures with the L^{SMe} Ligand. The ligands $L^{3,3',Me}$, $L^{5,3',Me}$, $L^{5,5',Me}$, L^{CF3}, L^{Br} were prepared to evaluate the influence of the functional groups of the pyrazole rings on the structural properties of the resulting coordination polymers. It was previously investigated how the modification of the peripheral thioether aromatic moiety would alter the structure and gas absorption capacity of hexameric assemblies (see Figure 1). By combining the results of these studies, it can be inferred that to obtain porous hexameric architecture, the sufficient condition is the presence of methyl groups in 3 and 5 positions on both the pyrazole rings. The nature of the peripheral group on the thioether moiety remained to be investigated because in all previous cases it was an aromatic system. The ligand L^{SMe} was therefore prepared to evaluate the effect of reducing the steric hindrance of the ligand with the purpose of increasing the porous capacity of putative hexameric species.

Two polymeric complexes were isolated by the reaction of $AgNO_3$ and $AgBF_4$ with L^{SMe}, and they both exhibit silver atoms in a distorted tetrahedral geometry achieved by two bidentate bispyrazolyl moieties. The thioether group then binds to an additional metal ion extending the polymeric structure demonstrated in Figure 8. The main difference between $[Ag(L^{SMe})]_n(NO_3)_n{\cdot}nCH_2Cl_2$ (**13**) and $[Ag_5(L^{SMe})_6]_n(BF_4)_{5n}$ (**14**) is in the overall framework generated, which depends on the number of metal−sulfur bonds present in the structures. In particular, in **13**, one of the two independent silver atoms interacts with two thioether groups and with two NO_3^- anion in a distorted tetrahedral environment. One of the nitrate anions, as well as the interacting silver cation, is statically disordered, and the geometry exhibited by this metal site is intermediate between the trigonal planar and tetrahedral. The resulting overall arrangement is in the form of a polymeric chain. On the other hand, in **14**, one of the metals is in a trigonal planar geometry deriving from three thioether groups. Two of the thioethers extend the assembly along one direction, analogously with the structure of **13**, whereas the third Ag−S interaction serves to link together two chains, thus forming a molecular ribbon. An asymmetric unit comprising five silver cations, six ligands, and five BF_4^- anions characterizes this complex. Three metals adopt a distorted tetrahedral geometry bound by two bidentate N,N ligands, whereas two metals adopt a trigonal planar geometry bound by three thioether groups. The quality of the data collection was not satisfactory for this structure, and the position and refinement of some of the anions are affected by some uncertainty. Nevertheless, above and below the trigonal plane of the S-bound silver atom are

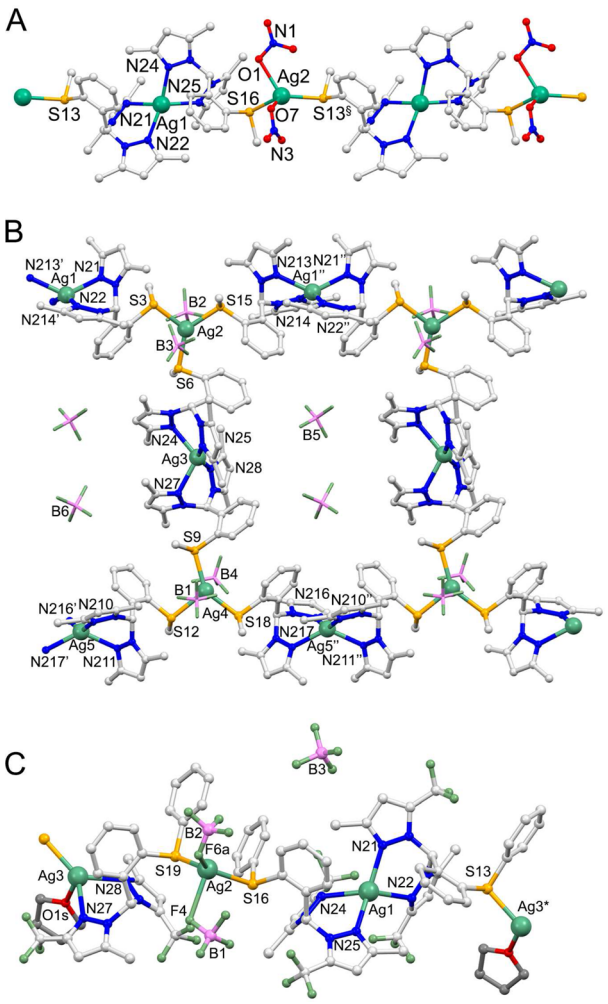

Figure 8. Molecular structures of the complexes for $[Ag(L^{SMe})]_n(NO_3)_n{\cdot}nCH_2Cl_2$ (**13**) (A), $[Ag_5(L^{SMe})_6]_n(BF_4)_{5n}$ (**14**) (B), and $[Ag_3(L^{CF3})_3(THF)]_n(BF_4)_{3n}$ (**15**) (C). Disordered anions, solvent molecules of crystallization, and hydrogen atoms were removed for clarity. Symmetry codes: § = *x*; *y*; 1 + *z*, ′ = 1 + *x*; *y*; *z*, ″ = *x* − 1; *y*; *z*, * = *x*; *y*; 2 + *z*.

located two BF_4^- anions, suggestive of the occurrence of a very weak type of interaction with the metal ion.

Interestingly, the ligand L^{CF3} also gave a molecular chain in the presence of $AgBF_4$ and after crystallization in the presence of a weakly coordination solvent such as THF, namely $[Ag_3(L^{CF3})_3(THF)]_n(BF_4)_{3n}$ (**15**). The structure is presented here because it exhibits similarities with those of L^{SMe}. However, when crystallizing the crude product in CH_2Cl_2, the complex $[Ag(L^{CF3})_2](BF_4){\cdot}CH_2Cl_2$ (**12**) described above was isolated. The complex **15** (Figure 8) is characterized by the presence of three types of silver atoms. Ag(1) exhibits a distorted tetrahedral geometry achieved by two N,N bidentate ligands, Ag(2) exhibits a distorted tetrahedral geometry and is bound by two thioether groups and two fluorine atoms of BF_4^- anions. Of the two Ag−F interactions, one is significantly shorter than the other (Ag(2)−F(6b)/F(7b) of approximately 2.4 Å and Ag(2)−F(4) of 2.64 Å). Finally, Ag(3) exhibits a distorted tetrahedral geometry according to the chelation of an N,N ligand, a bridging thioether, and the oxygen atom of the THF molecule. At variance with the structures with the L^{SMe} ligand, and in line with the presence of a peripheral aromatic

DOI: 10.1021/acs.cgd.6b00506
Cryst. Growth Des. XXXX, XXX, XXX−XXX

ring in L^{CF3}, there is a $\pi-\pi$ interaction between the two phenyl rings adjacent to the Ag(2) atom.

CONCLUSION

This paper reported the molecular structure of thioether-functionalized bis(pyrazolyl)methane complexes with Ag(I). The purpose of this work was to investigate the role of the structural modification on the ligand scaffold and evaluate its influence on the overall complex geometry. The work was inspired by recent findings that the change in the peripheral substituents could lead to cavity size modulation in microporous frameworks based on the same ligand class and with Ag(I).[41] Inspection of the crystal packing of these previously reported complexes clearly shows that two types of microporous structures were present and were surrounded by two ligand components. In particular, the larger cavity was lined with pyrazole methyl groups, whereas the smaller cavity was lined with the peripheral phenyl ring of the thioether moiety shown in Figure 9.

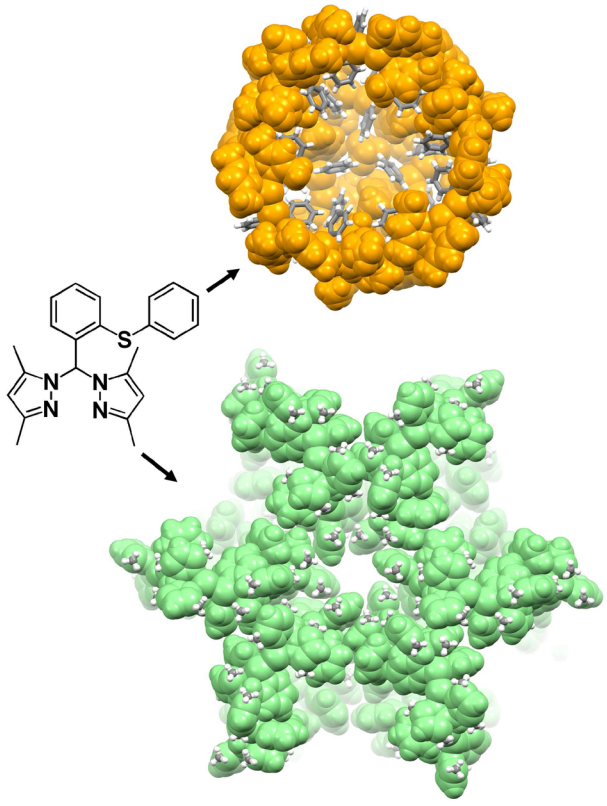

Figure 9. Depiction of the internal surface of the intracapsular (above) and intercapsular cavities of the $[Ag_6(L^{3,5})_6](BF_4)_6$ complex.[40,41]

The modification of the pyrazole substituents was investigated to lead to a modulation of the cavity size. Another interesting issue is related to the type of donor atoms surrounding the cavities, a fact that can have a strong impact on the absorption properties of a microporous material. The presence of F and Br atoms in L^{CF3} and L^{Br}, respectively, compared to the other ligands certainly modifies the selectivity index toward gaseous guests when a microporous material is obtained.[61−64] Nevertheless, in none of the reported compounds did the crystal packing exhibit a permanent porous structure. Fifteen structures are coordination polymers (molecular chains or grids, panels B and C in Figure 1), and seven structures are nonpolymeric (panels D and E in Figure 1). Some general observations can be drawn by inspecting the 30 structures of this ligand class with Ag(I) (see Figure 1). In particular, (1) the central phenyl ring provides a certain degree of ligand preorganization that favors a conformation in which the N_2 system and the thioether sulfur atom point in opposite directions, usually favoring a bridging ligand mode. This conclusion is supported by the occurrence of this ligand behavior in 23 out of 30 structures (compare panels A−C with D and E in Figure 1). This observation is also supported by the structures of similar bis(pyrazolyl)methane systems functionalized with a central aromatic moiety.[38,39,42,46,49,65−72] (2) The peripheral phenyl ring plays an important role as a source of various supramolecular interactions. In most of the cases it is involved in π-stacking, as in the case of the porous hexamers and the molecular chains, or it participates into CH$\cdots\pi$ interactions. The presence of the π-stacking with one of the pyrazole rings contributes to an additional ligand preorganization that may relevant to the formation of isostructural hexameric species. A depiction of the various ligands arrangements is summarized in Figure S10. The substitution of the phenyl group with a methyl one in L^{SMe} limits either the supramolecular interactions that can be exchanged by the ligand and it decreases significantly the steric hindrance. As an example, the absence of the aromatic ring in L^{SMe} allowed for the approach of three thioether groups toward a metal center in $[Ag_5(L^{SMe})_6]_n(BF_4)_{5n}$ (**14**, see Figure 8). (3) The effect of the methyl groups on the pyrazole rings can be appreciated by considering the structures with the ligands $L^{3,3',Me}$, $L^{5,5',Me}$, $L^{5,3',Me}$, L^{CF3}, and the parent ligand $L^{3,SMe}$. When the steric hindrance is removed from the N_2 donor system as in $L^{5,5',Me}$, dinuclear complexes can be formed because two AgL fragments can easily approach each other (see panel D in Figure 1). Furthermore, when a less symmetric steric hindrance occurs, as with $L^{5,3',Me}$, and L^{CF3}, it is more difficult to rationalize the structural outcome. In fact, CPs having the shape of helicoidal chains can be formed, as well as AgL_2 complexes, even though the synthesis was performed in the 1:1 M:L ratio (panel E of Figure 1). However, the four methyl groups in the parent ligand $L^{3,SMe}$ can provide a moderate steric hindrance stabilizing a specific ligand conformation in analogy the effect exerted by the central phenyl ring, thus resulting in the preferred formation of oligonuclear structures (porous hexamers). (4) The anion appears to have a significant influence on the resulting structural arrangement. In particular, the less symmetric but more coordinating triflate anion induces the formation of high nuclearity systems. In fact, out of the 10 reported structures with this anion, eight comprise an helicoidal molecular chain (irrespective of the pyrazole substituents: $L^{3,SMe}$, L^{Br}, $L^{5,3',Me}$, L^{CF3}), one is dinuclear and one is hexameric. The reason for this structural influence can be found in the coordination geometry of Ag(I) imposed by the triflate when compared to the less coordinated BF_4^- or PF_6^-. The presence of a N_2S donor ligand and the oxygen atom of the triflate anion tend to satisfy the requirement of Ag(I). In the presence of weakly coordinating anions such as BF_4^- or PF_6^-, however, the metal tends to satisfy its electronic requirements by binding to two N_2 systems and providing more varied molecular geometry, whose structural arrangements are driven by the aforementioned steric effect described in points (1)−(3). The combined effects of the anion properties and of the supramolecular interactions were investigated for other types of Ag(I) complexes, pointing to the

DOI: 10.1021/acs.cgd.6b00506
Cryst. Growth Des. XXXX, XXX, XXX−XXX

strength of the metal-anion interaction[73,74] or anion size[75] as key factors governing the overall architectures.

In conclusion, this work rationalizes the structural features of Ag(I) complexes with thioether functionalized bis(pyrazolyl)-methane ligands. Various effects dictate the resulting architectures, and the results based upon structural considerations can be valuable to direct future ligand modification to obtain a desired (porous) crystalline structure.

■ ASSOCIATED CONTENT

Supporting Information

The Supporting Information is available free of charge on the ACS Publications website at DOI: 10.1021/acs.cgd.6b00506.

Synthesis of the ligands and complexes, thermal ellipsoids plots of the asymmetric units of the Ag(I) coordination polymers, crystallographic tables (PDF)

Accession Codes

CCDC 1457814−1457828 contains the supplementary crystallographic data for this paper. These data can be obtained free of charge via www.ccdc.cam.ac.uk/data_request/cif, or by emailing data_request@ccdc.cam.ac.uk, or by contacting The Cambridge Crystallographic Data Centre, 12 Union Road, Cambridge CB2 1EZ, UK; fax: +44 1223 336033.

■ AUTHOR INFORMATION

Corresponding Author

*E-mail: marchio@unipr.it.

Present Address

[†]Dipartimento di Scienza dei Materiali, Università degli Studi di Milano Bicocca, via Roberto Cozzi 55, 20125, Milano, Italy.

Notes

The authors declare no competing financial interest.

■ ACKNOWLEDGMENTS

This study was supported by the Università degli Studi di Parma (Parma, Italy).

■ REFERENCES

(1) Cook, T. R.; Zheng, Y.; Stang, P. J. *Chem. Rev.* **2013**, *113*, 734−777.
(2) Cook, T. R.; Stang, P. J. *Chem. Rev.* **2015**, *115*, 7001−7045.
(3) Biradha, K.; Ramanan, A.; Vittal, J. J. *Cryst. Growth Des.* **2009**, *9*, 2969−2970.
(4) Moulton, B.; Zaworotko, M. J. *Chem. Rev.* **2001**, *101*, 1629−1658.
(5) Kitagawa, S.; Uemura, K. *Chem. Soc. Rev.* **2005**, *34*, 109−119.
(6) Du, M.; Banerjee, R.; Shimizu, G. K. H. *CrystEngComm* **2013**, *15*, 9237−9238.
(7) Robin, A. Y.; Fromm, K. M. *Coord. Chem. Rev.* **2006**, *250*, 2127−2157.
(8) Hasegawa, S.; Horike, S.; Matsuda, R.; Furukawa, S.; Mochizuki, K.; Kinoshita, Y.; Kitagawa, S. *J. Am. Chem. Soc.* **2007**, *129*, 2607−2614.
(9) Kajiwara, T.; Fujii, M.; Tsujimoto, M.; Kobayashi, K.; Higuchi, M.; Tanaka, K.; Kitagawa, S. *Angew. Chem., Int. Ed.* **2016**, *55*, 2697−2700.
(10) Flynn, D. C.; Ramakrishna, G.; Yang, H.; Northrop, B. H.; Stang, P. J.; Goodson, T., III *J. Am. Chem. Soc.* **2010**, *132*, 1348−1358.
(11) Cui, Y.; Yue, Y.; Qian, G.; Chen, B. *Chem. Rev.* **2012**, *112*, 1126−1162.
(12) Xie, Z.; Ma, L.; de Krafft, K. E.; Jin, A.; Lin, W. *J. Am. Chem. Soc.* **2010**, *132*, 922−923.
(13) Zhang, Q.; Li, B.; Chen, L. *Inorg. Chem.* **2013**, *52*, 9356−9362.
(14) Zhang, W.; Xiong, R. *Chem. Rev.* **2012**, *112*, 1163−1195.
(15) Gygi, D.; Bloch, E. D.; Mason, J. A.; Hudson, M. R.; Gonzalez, M. I.; Siegelman, R. L.; Darwish, T. A.; Queen, W. L.; Brown, C. M.; Long, R. *Chem. Mater.* **2016**, *28*, 1128−1138.
(16) Gándara, F.; Furukawa, H.; Lee, S.; Yaghi, O. M. *J. Am. Chem. Soc.* **2014**, *136*, 5271−5274.
(17) Ma, S.; Zhou, H. *Chem. Commun.* **2010**, *46*, 44−53.
(18) Barea, E.; Montoro, C.; Navarro, J. A. R. *Chem. Soc. Rev.* **2014**, *43*, 5419−5430.
(19) Bloch, D. E.; Queen, W. L.; Krishna, R.; Zadrozny, J. M.; Brown, C. M.; Long, J. R. *Science* **2012**, *335*, 1606−1611.
(20) Horcajada, P.; Gref, R.; Baati, T.; Allan, P. K.; Maurin, G.; Couvreur, P.; et al. *Chem. Rev.* **2012**, *112*, 1232−1268.
(21) Furukawa, H.; Cordova, K. E.; O'Keeffe, M.; Yaghi, O. M. *Science* **2013**, *341*, 1230444.
(22) Gao, W.; Chrzanowski, M.; Ma, S. *Chem. Soc. Rev.* **2014**, *43*, 5841−5866.
(23) Miras, H. N.; Vilà-Nadal, L.; Cronin, L. *Chem. Soc. Rev.* **2014**, *43*, 5679−5699.
(24) Atzeri, C.; Marchiò, L.; Chow, Y. C.; Kampf, J. W.; Pecoraro, V. L.; Tegoni, M. *Chem. - Eur. J.* **2016**, *22*, 6482−6486.
(25) Janiak, C.; Vieth, J. K. *New J. Chem.* **2010**, *34*, 2366−2388.
(26) Batten, S. R.; Champness, N. R.; Chen, X.; Garcia-martinez, J.; Kitagawa, S.; Ohrstrom, L.; et al. *CrystEngComm* **2012**, *14*, 3001−3004.
(27) Janiak, C. *Dalton Trans.* **2003**, 2781−2814.
(28) Kitagawa, S.; Kitaura, R.; Noro, S. *Angew. Chem., Int. Ed.* **2004**, *43*, 2334−2375.
(29) Puigmartí-luis, J.; Rubio-martínez, M.; Hartfelder, U.; Imaz, I.; Maspoch, D.; Dittrich, P. S. *J. Am. Chem. Soc.* **2011**, *133*, 4216−4219.
(30) Gómez-Herrero, J.; Zamora, F. *Adv. Mater.* **2011**, *23*, 5311−5317.
(31) Ohtani, R.; Inukai, M.; Hijikata, Y.; Ogawa, T.; Takenaka, M.; Ohba, M.; Kitagawa, S. *Angew. Chem., Int. Ed.* **2015**, *54*, 1139−1143.
(32) Khlobystov, A. N.; Blake, A. J.; Champness, N. R.; Lemenovskii, D. A.; Majouga, A. G.; Zyk, N. V.; Schröder, M. *Coord. Chem. Rev.* **2001**, *222*, 155−192.
(33) Carlucci, L.; Ciani, G.; Proserpio, D. M.; Rizzato, S. *CrystEngComm* **2002**, *4*, 121−129.
(34) Wu, H.; Dong, X.; Ma, J.; Liu, H.; Bai, H.; Yang, J. *Dalton Trans.* **2009**, 3162−3174.
(35) Caballero, A. B.; Maclaren, J. K.; Rodríguez-Diéguez, A.; Vidal, I.; Dobado, J. a.; Salas, J. M.; Janiak, C. *Dalton Trans.* **2011**, *40*, 11845−11855.
(36) Lu, X.; Ye, J.; Sun, Y.; Bogale, R. F.; Zhao, L.; Tian, P.; Ning, G. *Dalton Trans.* **2014**, *43*, 10104−10113.
(37) Serpe, A.; Artizzu, F.; Marchiò, L.; Mercuri, M. L.; Pilia, L.; Deplano, P. *Cryst. Growth Des.* **2011**, *11*, 1278−1286.
(38) Bassanetti, I.; Marchio, L. *Inorg. Chem.* **2011**, *50*, 10786−10797.
(39) Gennari, M.; Bassanetti, I.; Marchio, L. *Polyhedron* **2010**, *29*, 361−371.
(40) Bassanetti, I.; Mezzadri, F.; Comotti, A.; Sozzani, P.; Gennari, M.; Calestani, G.; Marchiò, L. *J. Am. Chem. Soc.* **2012**, *134*, 9142−9145.
(41) Bassanetti, I.; Comotti, A.; Sozzani, P.; Bracco, S.; Calestani, G.; Mezzadri, F.; Marchio, L. *J. Am. Chem. Soc.* **2014**, *136*, 14883−14895.
(42) Reger, D. L.; Watson, R. P.; Smith, M. D.; Pellechia, P. J.; October, R. V. *Organometallics* **2006**, *25*, 743−755.
(43) Reger, D. L.; Foley, E. A.; Smith, M. D. *Inorg. Chem.* **2010**, *49*, 234−242.
(44) Zhang, L.; Ren, Z.; Li, H.; Lang, J. *CrystEngComm* **2011**, *13*, 1400−1405.
(45) Reger, D. L.; Watson, R. P.; Gardinier, J. R.; Smith, M. D. *Inorg. Chem.* **2004**, *43*, 6609−6619.
(46) Gardinier, J. R.; Tatlock, H. M.; Hewage, J. S.; Lindeman, S. V. *Cryst. Growth Des.* **2013**, *13*, 3864−3877.
(47) Reger, D. L.; Pascui, A. E.; Smith, M. D. *Eur. J. Inorg. Chem.* **2012**, *2012*, 4593−4604.
(48) Morin, T. J.; Merkel, A.; Lindeman, S. V.; Gardinier, J. R. *Inorg. Chem.* **2010**, *49*, 7992−8002.

DOI: 10.1021/acs.cgd.6b00506
Cryst. Growth Des. XXXX, XXX, XXX−XXX

(49) Santillan, G. A.; Carrano, C. J. *Inorg. Chem.* **2007**, *46*, 1751−1759.
(50) Dura, G.; Manzano, B. R.; Carrión, M. C.; Jalón, F. A.; Rodriguez, A. M. *Cryst. Growth Des.* **2014**, *14*, 3510−3529.
(51) Chandrasekhar, V.; Thilagar, P.; Senapati, T. *Eur. J. Inorg. Chem.* **2007**, *2007*, 1004−1009.
(52) Reger, D. L.; Brown, K. J.; Gardinier, J. R.; Smith, M. D. *Organometallics* **2003**, *22*, 4973−4983.
(53) Gardinier, J. R.; Hewage, J. S.; Lindeman, S. V. *Inorg. Chem.* **2014**, *53*, 1975−1988.
(54) Gilday, L. C.; Robinson, S. W.; Barendt, T. A.; Langton, M. J.; Mullaney, B. R.; Beer, P. D. *Chem. Rev.* **2015**, *115*, 7118−7195.
(55) *SMART (control) and SAINT (integration) Software for CCD Systems*; Bruker AXS: Madison, WI, 1994.
(56) *Area-Detector Absorption Correction*; Siemens Industrial Automation Inc.: Madison, WI, 1996.
(57) Burla, M. C.; Caliandro, R.; Camalli, M.; Carrozzini, B.; Cascarano, G. L.; De Caro, L.; Giacovazzo, C.; Polidori, G.; Spagna, R. *J. Appl. Crystallogr.* **2005**, *38*, 381−388.
(58) Sheldrick, G. M. *Acta Crystallogr., Sect. A: Found. Crystallogr.* **2008**, *64*, 112−122.
(59) Farrugia, L. J. *J. Appl. Crystallogr.* **1999**, *32*, 837−838.
(60) Macrae, C. F.; Edgington, P. R.; McCabe, P.; Pidcock, E.; Shields, G. P.; Taylor, R.; Towler, M.; van de Streek, J. *J. Appl. Crystallogr.* **2006**, *39*, 453−457.
(61) Ni, J.; Wei, K.-J.; Liu, Y.; Huang, X.-C.; Li, D. *Cryst. Growth Des.* **2010**, *10*, 3964−3976.
(62) Yang, C.; Kaipa, U.; Mather, Q. Z.; Wang, X.; Nesterov, V.; Venero, A. F.; Omary, M. A. *J. Am. Chem. Soc.* **2011**, *133*, 18094−18097.
(63) Hulvey, Z.; Sava, D. A.; Eckert, J.; Cheetham, A. K. *Inorg. Chem.* **2011**, *50*, 403−405.
(64) Li, J.-R.; Kuppler, R. J.; Zhou, H. *Chem. Soc. Rev.* **2009**, *38*, 1477−1504.
(65) Reger, D. L.; Pascui, A. E.; Foley, E. A.; Smith, M. D.; Jezierska, J.; Ozarowski, A. *Inorg. Chem.* **2014**, *53*, 1975−1988.
(66) Pilar Carranza, M.; Manzano, B. R.; Jalón, F. a.; Rodríguez, A. M.; Santos, L.; Moreno, M. *New J. Chem.* **2013**, *37*, 3183−3194.
(67) Santillan, G. A.; Carrano, C. J. *Inorg. Chem.* **2008**, *47*, 930−939.
(68) Reger, D. L.; Pascui, A. E.; Smith, M. D.; Jezierska, J.; Ozarowski, A. *Inorg. Chem.* **2012**, *51*, 11820−11836.
(69) Willis, C.; Messerle, B. A.; Ho, J. H. H.; Wagler, J. *Dalton Trans.* **2011**, *40*, 11031−11042.
(70) Reger, D. L.; Watson, R. P.; Smith, M. D. *Inorg. Chem.* **2006**, *45*, 10077−10087.
(71) Santillan, G. A.; Carrano, C. J. *Dalton Trans.* **2008**, 3995−4005.
(72) Wang, S.; Zang, H.; Sun, C.; Xu, G.; Wang, X.; Shao, K.; Lan, Y.; Su, Z. *CrystEngComm* **2010**, *12*, 3458−3462.
(73) Co, C. F.; So, C. F.; Jung, O.; Kim, Y. J.; Lee, Y.; Park, K.; Lee, S. S. *Inorg. Chem.* **2003**, *42*, 844−850.
(74) Lee, E.; Ju, H.; Kim, S.; Park, K.; Lee, S. S. *Cryst. Growth Des.* **2015**, *15*, 5427−5436.
(75) Andreychuk, N. R.; Allard, S. R.; Parent, S. L. M.; Assoud, A.; Mackinnon, C. D. *Cryst. Growth Des.* **2015**, *15*, 4377−4384.

DOI: 10.1021/acs.cgd.6b00506
Cryst. Growth Des. XXXX, XXX, XXX−XXX